Magnetic Resonance Imaging 31 (2013) 466–476

Contents lists available at SciVerse ScienceDirect

Magnetic Resonance Imaging

journal homepage: www.mrijournal.com

Performance evaluation of nonnegative matrix factorization algorithms to estimate task-related neuronal activities from fMRI data ☆

Xiaoyu Ding [a], Jong-Hwan Lee [b], Seong-Whan Lee [b,*]

[a] Department of Computer Science and Engineering, Korea University, Anam-dong, Seongbuk-ku, Seoul 136-713, Korea
[b] Department of Brain and Cognitive Engineering, Korea University, Anam-dong, Seongbuk-ku, Seoul 136-713, Korea

ARTICLE INFO

Article history:
Received 18 December 2011
Revised 4 September 2012
Accepted 14 October 2012

Keywords:
Nonnegative matrix factorization (NMF)
Blind source separation (BSS)
Functional magnetic resonance imaging (fMRI)
Visuomotor task

ABSTRACT

Nonnegative matrix factorization (NMF) is a blind source separation (BSS) algorithm which is based on the distinct constraint of nonnegativity of the estimated parameters as well as on the measured data. In this study, according to the potential feasibility of NMF for fMRI data, the four most popular NMF algorithms, corresponding to the following two types of (1) least-squares based update [i.e., alternating least-squares NMF (ALSNMF) and projected gradient descent NMF] and (2) multiplicative update (i.e., NMF based on Euclidean distance and NMF based on divergence cost function), were investigated by using them to estimate task-related neuronal activities. These algorithms were applied firstly to individual data from a single subject and, subsequently, to group data sets from multiple subjects. On the single-subject level, although all four algorithms detected task-related activation from simulated data, the performance of multiplicative update NMFs was significantly deteriorated when evaluated using visuomotor task fMRI data, for which they failed in estimating any task-related neuronal activities. In group-level analysis on both simulated data and real fMRI data, ALSNMF outperformed the other three algorithms. The presented findings may suggest that ALSNMF appears to be the most promising option among the tested NMF algorithms to extract task-related neuronal activities from fMRI data.

1. Introduction

Functional magnetic resonance imaging (fMRI) has been widely adopted as a noninvasive method to explore brain function based on blood oxygenation level-dependent (BOLD) signal variation associated with the neuronal activity. The methods applied in analyzing fMRI data were dominated by model-based approaches (e.g., GLM [1]) in the early years. These approaches assume the hemodynamic response function (HRF) to be known and then model a regressor using the given HRF to estimate the most likely voxel response. However, the modeled regressor may not represent the exact changes in BOLD signals. Also, it is difficult to model a regressor for some experiments.

In this case, data-driven approaches have been introduced and widely adopted in the last decade. Data-driven methods treat fMRI data in the context of a blind source separation (BSS) problem, which does not need any kinds of prior information to produce both time courses and spatial maps. Multivariate approaches have been proposed with regard to the BSS problem. Some representative multivariate BSS algorithms regarding fMRI analysis are principal component analysis (PCA) [2], independent component analysis (ICA) [3], independent vector analysis [4] and canonical correlation analysis [5]. Among these, ICA together with a PCA dimension reduction step [6] is the most commonly used BSS approach. It finds statistically independent components in a subspace that has been obtained using PCA. Previous studies have proved that this approach can yield meaningful and reliable components [7–10]. As there are several kinds of ICA algorithms (e.g., Infomax, FastICA, Jade) based on different optimization approaches to get independent components, the performances of these different ICA algorithms were evaluated in previous research studies [10]. The other BSS algorithms, although were rarely applied in fMRI studies, were also explored by researchers. For example, in Ref. [11], the author evaluated the performance of three factor analysis algorithms on fMRI data in both the spatial and temporal domains.

A previous literature indicated that the validity of ICA algorithms on fMRI data was linked to their ability in handling the sparse components effectively [12]. From this point of view, nonnegative matrix factorization (NMF) is a potentially viable data-driven multivariate analytical option, as it decomposes nonnegative datasets into a linear combination of sparse and part-based nonnegative features. Taking its well-known application on facial images for example, it decomposes a dataset of

☆ This research was supported in part by the World Class University (WCU) Program through the National Research Foundation of Korea funded by the Ministry of Education, Science, and Technology, under Grant R31-10008; and in part by the Korea Science and Engineering Foundation (KOSEF) Grant funded by the Ministry of Education, Science, and Technology, under Grant 2012-005741.

* Corresponding author. Department of Brain and Cognitive Engineering, Korea University, Anam-dong, Seongbuk-ku, Seoul 136-713, Korea. Tel.: +82 2 3290 3197; fax: +82 2 3290 3583.
E-mail addresses: xyding@image.korea.ac.kr (X. Ding), jonghwan_lee@korea.ac.kr (J-H. Lee), swlee@image.korea.ac.kr (S-W. Lee).

0730-725X/$ – see front matter © 2013 Elsevier Inc. All rights reserved.
http://dx.doi.org/10.1016/j.mri.2012.10.003

face images into a set of sparse features representing connotative parts such as mouth, nose and eyes [13,14]. It has also been widely applied in many other areas, including biomedical applications, e.g., encoding the electric neuronal activity [14], characterization of genetic types [15] and tumor classification [16]. Also, there are several studies that have introduced NMF into the field of fMRI study [17–20]. Among these, Refs. [17] and [19] introduced NMF to analyze fMRI time series. Ref. [17] was a region of interest (ROI) analysis that analyzed BOLD time series in a specific brain region, whereas Ref. [19] was a data-driven multivariate approach which pays more attention to finding a whole brain neuronal activity map.

For this wide range of applications of the NMF method, and inspired by its potential feasibility for fMRI data, we did an exploratory experiment that investigated the performance of four basic NMF algorithms with two different types of updating rules in estimating task-related neuronal activities from fMRI data. They were primarily assessed on the single subject level and, later, on the group level for both simulated data and visuomotor task fMRI data. The rest of this article is organized as follows: Section 2 describes the materials and methods used in our experiment; it contains a short review of NMF algorithms and a description of the data sets and the experimental steps. Section 3 presents experimental results revealing the performance of different NMF algorithms. We discuss a little bit more elaborately the interesting aspects of the work in Section 4 and give a conclusion in Section 5.

2. Materials and methods

2.1. Nonnegative matrix factorization algorithms

NMF is an algorithm that decomposes a 2D nonnegative input data matrix into two nonnegative output matrices with a reduced number of parameters compared to the original input data, which provides an option to obtain an efficient feature extraction. The NMF model can be expressed as

$$\mathbf{X}\approx\mathbf{WH} \tag{1}$$

Here, the input nonnegative matrix **X** of size $M\times N$ (where M is the number of input vectors and N is the number of elements in each input vector) is decomposed into an $M\times K$ nonnegative weight matrix **W** and a $K\times N$ nonnegative basis matrix **H**, where K is the number of basis (usually $K<MN/(M+N)$ [13]).

The earliest version of NMF was proposed by Paatero and Tapper [21] under the name of positive matrix factorization. They refined it in Ref. [22] by using a constraint of nonnegativity instead of positivity. Later, Lee et al. proposed their NMF algorithms which used multiplicative update rules in 1999 [13] and in 2001 [23]. Lin [24] proposed a least squares with projected gradient method for NMF. A number of researchers appended additional constraints such as sparseness to the nonnegative property in order to improve the performance of the feature extraction or algorithm stability, e.g., Refs. [14,25–27]. In general, almost all derivative forms of NMF originate from two NMF groups containing four popular algorithms described in detail as follows.

2.1.1. Group 1: Least-squares update NMF

2.1.1.1. Alternating least-squares NMF. Alternating least-squares NMF (ALSNMF) [22] finds **W** and **H** by minimizing the Euclidean distance between **X** and **WH**:

$$\min_{\mathbf{W},\mathbf{H}} f(\mathbf{W},\mathbf{H})=\frac{1}{2}||\mathbf{X}-\mathbf{WH}||^2, \text{w.r.t.},\ W_{ij}\geq 0, H_{ij}\geq 0, \forall i,j \tag{2}$$

The solution of this problem, which is overdetermined due to the greater number of observations (i.e., input data) compared to the number of basis to be estimated, is derived from the least-squares solutions. Particularly, each of the two parameters (i.e., **W** and **H**) is iteratively updated using the remaining parameter with its most recent values in each by a least-squares step:

$$\mathbf{W}=\left[\mathbf{X}\mathbf{H}^{\mathrm{T}}\left(\mathbf{H}\mathbf{H}^{\mathrm{T}}\right)^{-1}\right]_{+}, \mathbf{H}=\left[\left(\mathbf{W}^{\mathrm{T}}\mathbf{W}\right)^{-1}\mathbf{W}^{\mathrm{T}}\mathbf{X}\right]_{+} \tag{3}$$

where $[x]_+=\max\{0,x\}$ denotes setting all negative elements in x to 0.

This approach is the "block coordinate descent" method in a bound-constrained optimization [24], where one block is fixed and the other block of variables is minimized under corresponding nonnegative constraints.

2.1.1.2. Projected gradient descent NMF. Projected gradient descent NMF minimizes the Euclidean distance cost function Eq. (2) by taking a step size approach in the direction of steepest descent to find a stable and convergent point for both **W** and **H**. It is a gradient descent least-squares method. A general form is shown as follows:

$$\mathbf{W}=\left[\mathbf{W}-\varepsilon_{\mathrm{W}}(\mathbf{WH}-\mathbf{X})\mathbf{H}^{\mathrm{T}}\right]_{+}, \mathbf{H}=\left[\mathbf{H}-\varepsilon_{\mathrm{H}}\mathbf{W}^{\mathrm{T}}(\mathbf{WH}-\mathbf{X})\right]_{+} \tag{4}$$

A representative method proposed by Lin [24] adaptively changes the scalar values of learning rates, i.e., ε_{W} andε_{H}, to ensure sufficient minimization of the cost function. In our experiment, Lin's algorithm was employed; it is denoted as cjlinNMF in the remaining parts of this article.

2.1.2. Group 2: Multiplicative update NMF

2.1.2.1. Multiplicative update NMF based on the Euclidean distance cost function. Lee et al. [13] proposed an NMF algorithm using multiplicative update rules based on the Euclidean distance cost function Eq. (2) in 1999. It is simple to implement. The elements of **W** and **H** are multiplied by certain factors as follows:

$$w_{ij}=w_{ij}\frac{\left[\mathbf{X}\mathbf{H}^{\mathrm{T}}\right]_{ij}}{\left[\mathbf{W}\mathbf{H}\mathbf{H}^{\mathrm{T}}\right]_{ij}}, h_{jt}=h_{jt}\frac{\left[\mathbf{W}^{\mathrm{T}}\mathbf{X}\right]_{jt}}{\left[\mathbf{W}^{\mathrm{T}}\mathbf{W}\mathbf{H}\right]_{jt}} \tag{5}$$

As there is no negative element in the original input data matrix, and also because the zero elements of **W** and **H** are not updated during iterations, the above update rules ensure that all the elements in **W** and **H** are strictly nonnegative for all iterations. We abbreviate this multiplicative update NMF algorithm as eucNMF in this article.

2.1.2.2. Multiplicative update NMF based on a divergence cost function. In 2001, the same authors, Lee et al. [23], proposed another multiplicative update NMF taking the Kullback–Leibler divergence as its cost function in the following form:

$$\min_{\mathbf{W},\mathbf{H}} D_{\mathrm{KL}}(\mathbf{X}||\mathbf{WH}) = \sum_{it}\left(x_{it}\ln\frac{x_{it}}{[\mathbf{WH}]_{it}}-x_{it}+[\mathbf{WH}]_{it}\right), \text{w.r.t.}, W_{ij}\geq 0, H_{ij}\geq 0, \forall i,j \tag{6}$$

Strictly speaking, it is a form of positive matrix factorization, as the Kullback–Leiber divergence cost function is not well defined if any x_{it} or $[\mathbf{WH}]_{it}$ is equal to 0. The deduced update rules are:

$$w_{ij}=w_{ij}\frac{\sum_{t=1}^{\mathrm{T}}h_{jt}\left(x_{it}/[\mathbf{WH}]_{it}\right)}{\sum_{t=1}^{\mathrm{T}}h_{jt}}, h_{jt}=h_{jt}\frac{\sum_{i=1}^{I}w_{ij}\left(x_{it}/[\mathbf{WH}]_{it}\right)}{\sum_{i=1}^{I}w_{ij}} \tag{7}$$

In order to distinguish it from eucNMF, this multiplicative update NMF is referred to as divNMF through the article.

2.2. Data and analysis

For fMRI data, the NMF model can be illustrated by Fig. 1. The input data matrix **X** is the BOLD matrix. The *i*th row in the basis matrix **H** represents the *i*th spatial map, and the *i*th column in the weight matrix **W** can be viewed as a time course corresponding to the *i*th spatial map in **H**. In Fig. 1, according to the non-negativity property of NMF algorithms, the decomposed spatial map matrix and time course matrix are both nonnegative. They can be viewed as positive baseline's biased matrices, i.e., each spatial map or time course is biased with its individual positive baseline. After subtracting the baseline from corresponding spatial map or time course, it will have zero mean with both positive and negative values.

In order to evaluate the performance of NMF algorithms, we conducted an evaluation experiment in which the algorithms were used to estimate task-related neuronal activities from the single subject and a group of multiple subjects using both simulated data and real fMRI data.

2.2.1. Generation of simulated data

Fig. 2 shows the simulated data which were generated according to the model:

$$D = T_A \times S_A + T_B \times S_B + C + N \tag{8}$$

S_A and S_B represented two source spatial maps (both have a size of 30×30 pixels) related to tasks *A* and *B*. Both S_A and S_B contained two activations in positive intensity and one deactivation denoted by a negative value. All activations and deactivation were in size of 4×4 pixels. The spatial maps were convolved with a smooth kernel matrix to get smoothing. Two different time courses, denoted by T_A and T_B, which were obtained by convolving 120 time points with an HRF corresponded to S_A and S_B, respectively. Then the spatial maps S_A and S_B were reshaped into row vectors and mixed with the time courses T_A and T_B, resulting in a 120×900 mixed dataset. The ultimate dataset *D* was obtained by adding a positive constant *C* which represents the baseline signal and a zero mean Gaussian noise *N* with the contrast-to-noise ratio of 3.9. We generated data for 15 subjects with randomly assigned baseline levels and Gaussian noise. All the data were checked to ensure their nonnegativity.

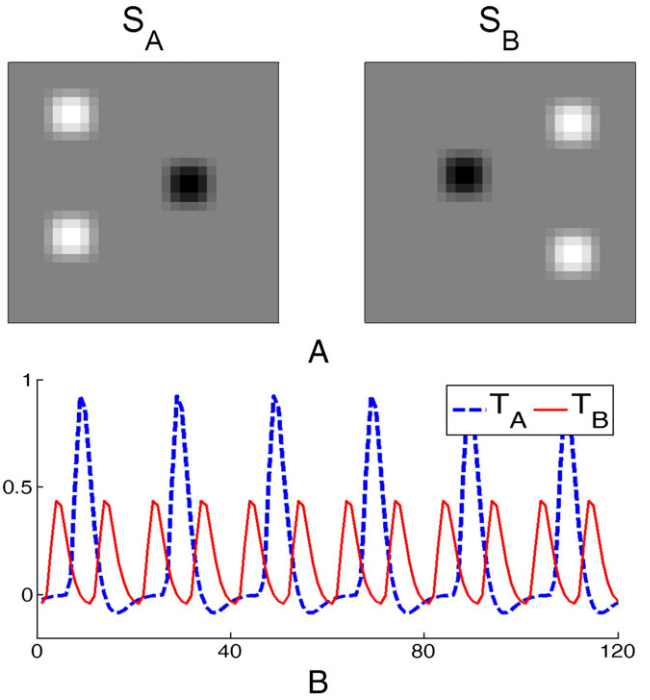

Fig. 2. Simulated data: (A) task-related spatial maps, where the white blocks indicate the activation and the black blocks denote the deactivation; (B) task-related time courses.

2.2.2. Real fMRI data and preprocessing

We used Buckner's fMRI dataset [28] downloaded from fMRIDC (http://www.fmridc.org, accession no. 2-2000-1118 W). The data were recorded from 14 young participants, as well as 14 non-demented and 13 demented older participants, performing one-trial and two-trial pseudo-randomly intermixed visuomotor tasks. The basic task paradigm was that participants pressed a key with their right index fingers upon the onset of a visual stimulus of 1.5 s duration. The visual stimulus was an 8-Hz counter-phase flickering (black to white) checkerboard subtending 12° of visual angle [28]. The one-trial condition indicated that the stimulus was presented in

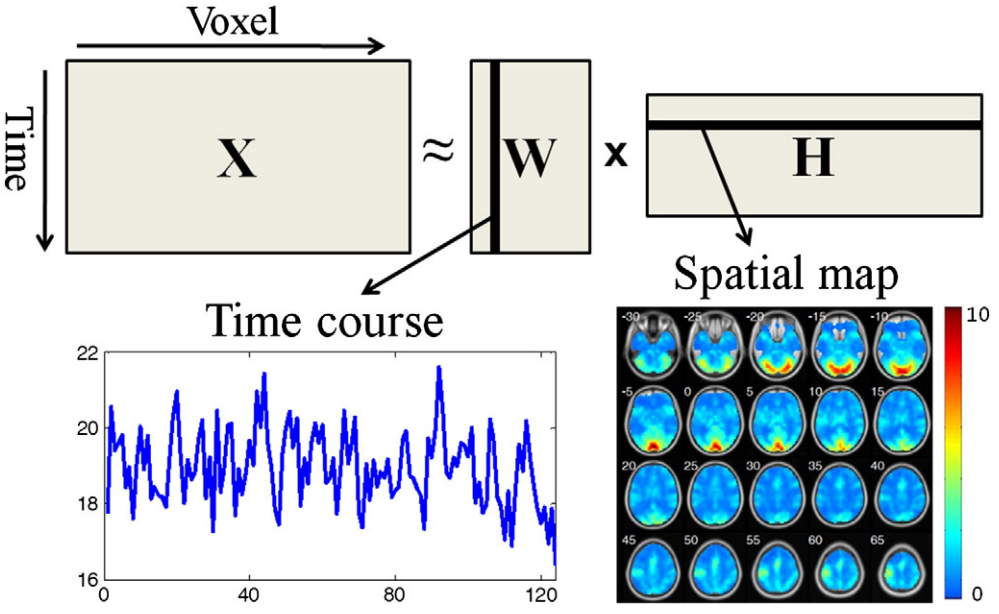

Fig. 1. NMF model for fMRI data.

isolation in a task trial, while the two-trial condition involved a pair of stimuli with an inter-trial interval of 5.36 s in a task trial. The functional images were acquired by using a Siemens 1.5-T Vision System (Erlangen, Germany) with the following parameters: repeat time=2.68 s, echo time=37 ms, field of view=24 cm, acquisition matrix=64×64, flip angle=90°, slice thickness=8 mm, involving 16 contiguous slices with interleaved sequence order. For each subject, 4 separate runs with 15 trials per run were recorded, yielding 128 sequential whole-brain image acquisitions for each run.

We took the 14 young subjects' run01 data for our experiment. As there was no dummy scan performed at the beginning, the first four image volumes were discarded to allow longitudinal equilibrium. The data were preprocessed by SPM8 (http://www.fil.ion.ucl.ac.uk/spm/software/spm8/) according to the typical fMRI preprocessing procedure: slice timing differences were corrected for each volume, and the volumes were realigned for movement correction. Then data were spatially normalized into the standard Montreal Neurological Institute (MNI) space with 3-mm isotropic voxels and smoothed with an 8-mm^3 full-width at half-maximum Gaussian kernel, resulting in 53×63×46 voxels. The experimental paradigm of run01 is illustrated in Fig. 3. We then convolved it with an assumed HRF to obtain the modeled task-related regressor of run01 for later use.

2.2.3. Application of NMF to simulated data and real fMRI data

NMF algorithms were applied to both simulated data and real fMRI data to carry out single-subject level and group-level analysis. In order to ensure the nonnegative property, as well as to coordinate with the conventional application approaches of the NMF algorithms [13–16], no additional preprocessing step (e.g., centering) was performed on the input data matrix.

In the single-subject level analysis, we first ran NMF algorithms on each individual dataset separately (dataset size: 120×900 for simulated data, 124×64343 for fMRI BOLD matrix), resulting in a time course matrix and a spatial map matrix for each subject. In the training process, the time courses were scaled to unit variance, and the corresponding spatial patterns were scaled in the opposite direction to ensure that the product of **W** and **H** remained the same. The number of components was set to three for the simulated data, with a prior knowledge that we generated two task-related components and one Gaussian noise component. For fMRI data, the number of components was set to 10 by experience. For each subject and each algorithm, the task-related component was selected as the one whose time course exhibited the highest correlation with the previously modeled regressor. The spatial pattern of the task-related component was transformed into *z*-scores of zero mean and unit variance [3,6,7] (i.e., $z = (x-\mu)/\sigma$, where x is the value of each voxel in a selected spatial map, μ and σ are the mean and standard deviation of this spatial map). As the time courses had already been scaled to unit variance in previous NMF training, the selected task-related time course was only shifted to zero mean to complete the *z*-score calculation. This *z*-score transformation step made the previous nonnegative time courses and spatial maps reveal positive values as well as negative ones. Then a random-effect analysis using a one-sample *t* test was performed on these *z*-scored spatial maps to infer the group-level activation pattern. The corresponding task-related time courses from each subject were averaged. Additionally, we evaluated the reproducibility for both estimated spatial and temporal patterns for those algorithms that effectively estimated the task-related neuronal activities, by applying each algorithm 20 times to each subject's fMRI data.

To apply the algorithms to data from a group of multiple subjects, an ad hoc procedure using a temporal concatenation [6] was adopted, in which subjects' data matrices were temporally concatenated to form a group-level 2D matrix (1800×900 for the simulated data and 1736×64,343 for the fMRI BOLD matrix). In order to eliminate subject discrepancy caused by distinct baseline

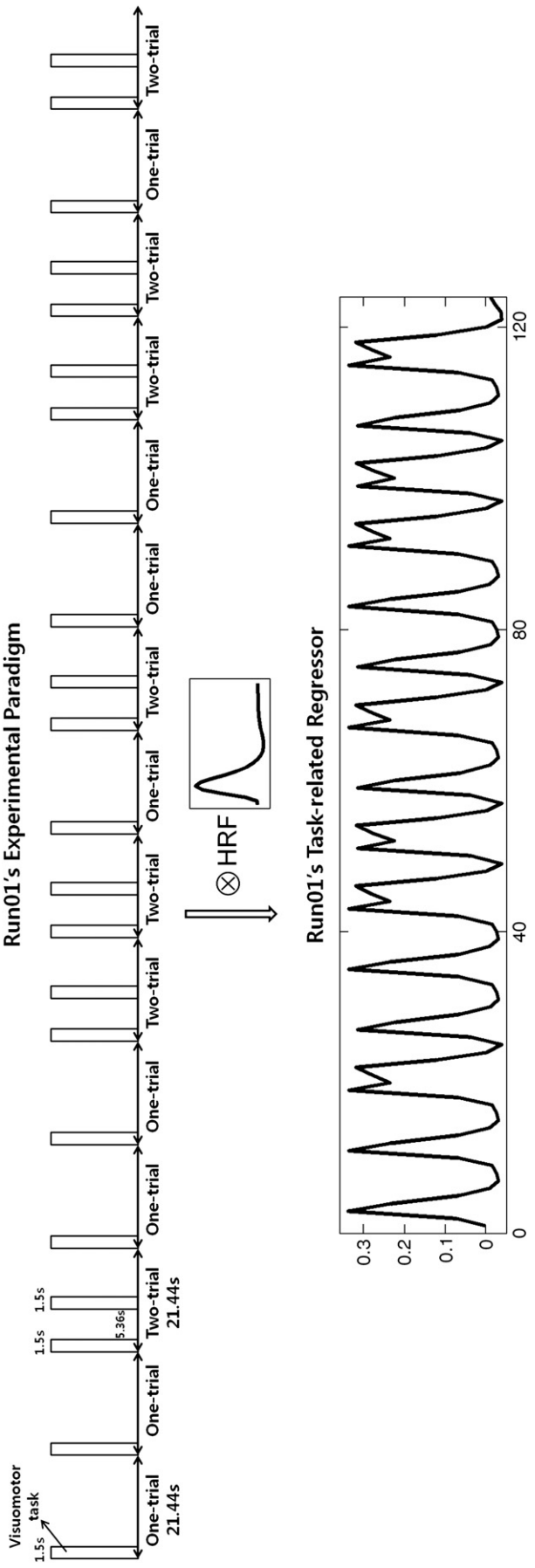

Fig. 3. Experimental paradigm and modeled task-related regressor.

signals, we removed the mean from each subject's data before temporal concatenation, then added the same randomly assigned baseline level to each subject's data to ensure nonnegativity. The goal of this temporal concatenation was to estimate the common spatial maps shared by all subjects at the group level, together with the corresponding subject-level time courses with differences among subjects. The NMF algorithms were applied to the concatenated 2D matrix. The number of components was still fixed at three for the simulated data, while for the fMRI data, taking the huge data size into consideration, the number of components

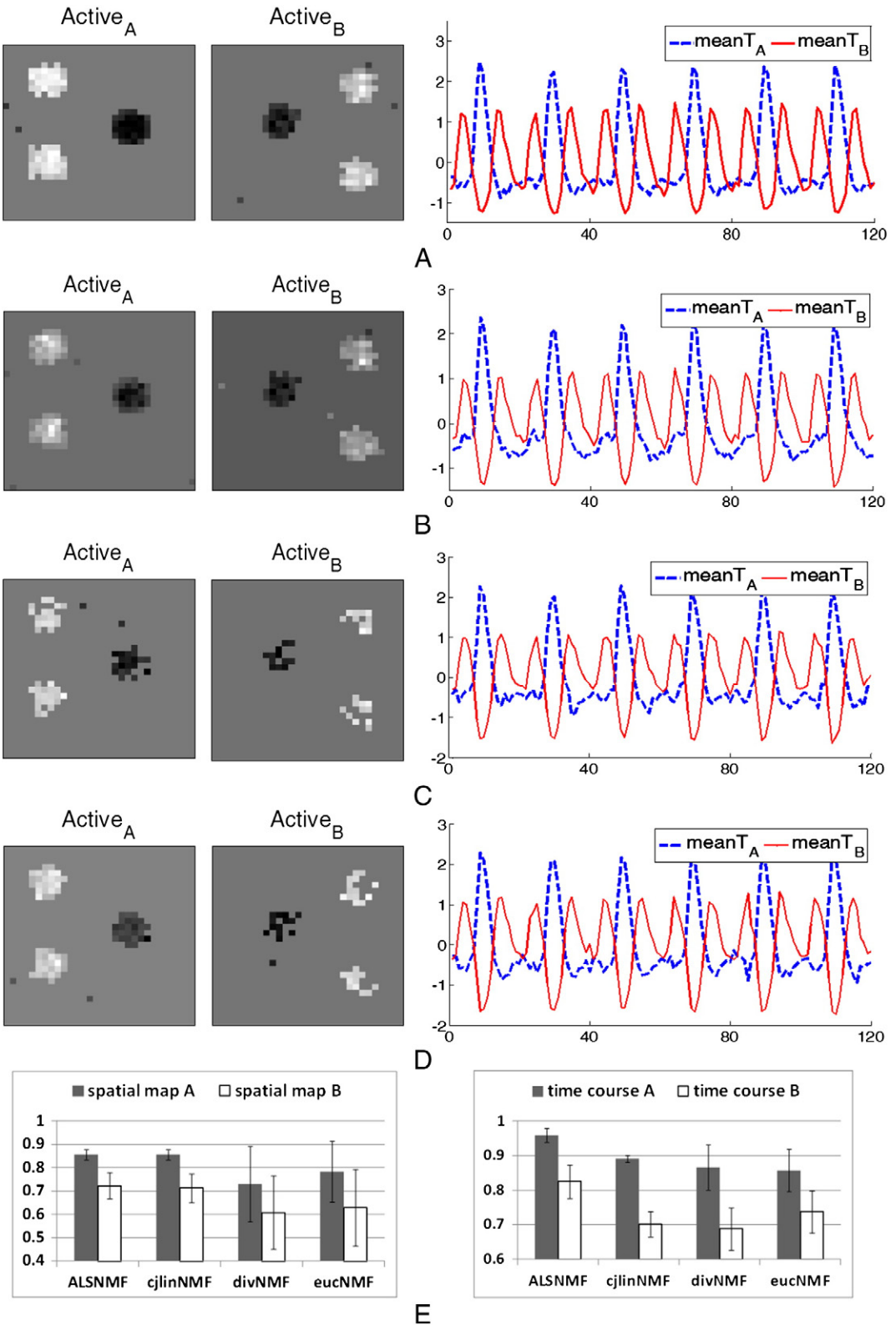

Fig. 4. Single-subject level results for simulated data: (A–D) Detected activation and deactivation (P<1e−5), as well as time courses obtained using (A) ALSNMF, (B) cjlinNMF, (C) divNMF and (D) eucNMF; (E) Pearson's correlation of spatial and temporal patterns from each subject with the reference.

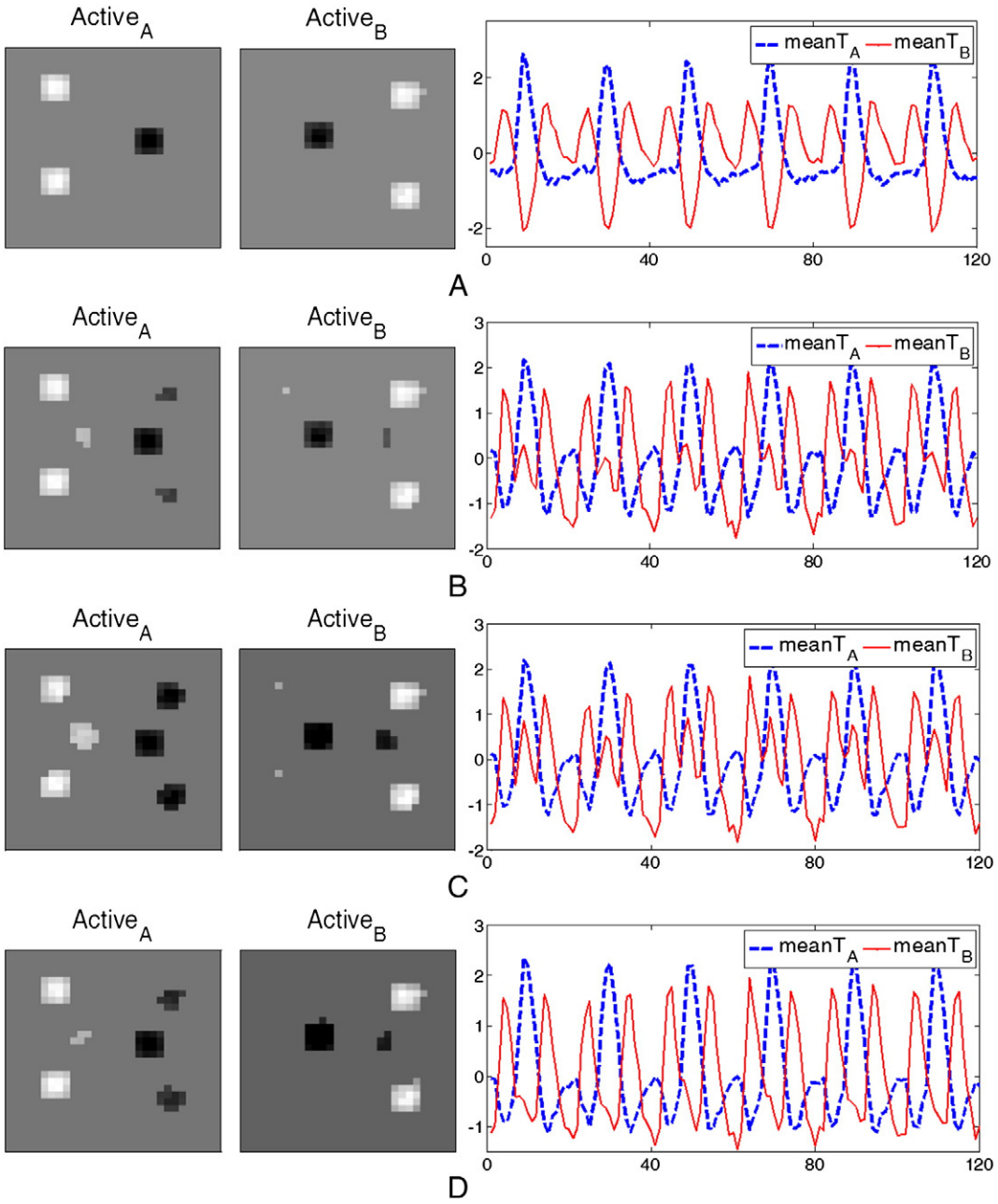

Fig. 5. Group-level results for simulated data: (A–D) Detected activation and deactivation ($|z|>2.0$), as well as time courses obtained using (A) ALSNMF, (B) cjlinNMF, (C) divNMF and (D) eucNMF.

was changed to 29 based on minimum description length (MDL) criteria [29]. The time course matrix was separated into individual time courses and normalized to have zero mean and unit variance. Then a mean time course was calculated for each component. For fMRI data, the task-related component was also selected with the aid of the modeled regressor. The associated spatial map was then converted to a *z*-score map. Voxels with their absolute *z*-scores greater than some threshold were considered as active voxels [3,7].

In order to make a comparison of the NMF algorithms, reference spatial and temporal patterns were designed: for artificial data, the simulated spatial maps and time courses were directly used as ground truth. The reference spatial and temporal patterns for real fMRI data were adopted from the results of Infomax using the same data sets under the same experimental settings (e.g., number of components) due to the confirmation of Infomax's reliability by previous research studies [7–10]. Pearson's correlation coefficients were used to measure the performance of the estimated spatial and temporal patterns. Furthermore, we created masks of task-related appropriate Brodmann areas (BAs) [8]: BAs 1, 2, 3, 4 and 6 in the left hemisphere, which include left-side somatosensory and motor areas; BAs 17, 18 and 19 in both hemispheres containing the visual

Table 1
Pearson's correlation with the reference for simulated data in the group analysis

	Spatial map A	Spatial map B	Time course A	Time course B
ALSNMF	0.9747	0.9497	0.9977	0.8924
cjlinNMF	0.8790	0.8924	0.8916	0.8948
divNMF	0.7387	0.8480	0.9070	0.7790
eucNMF	0.8506	0.8797	0.9486	0.9820

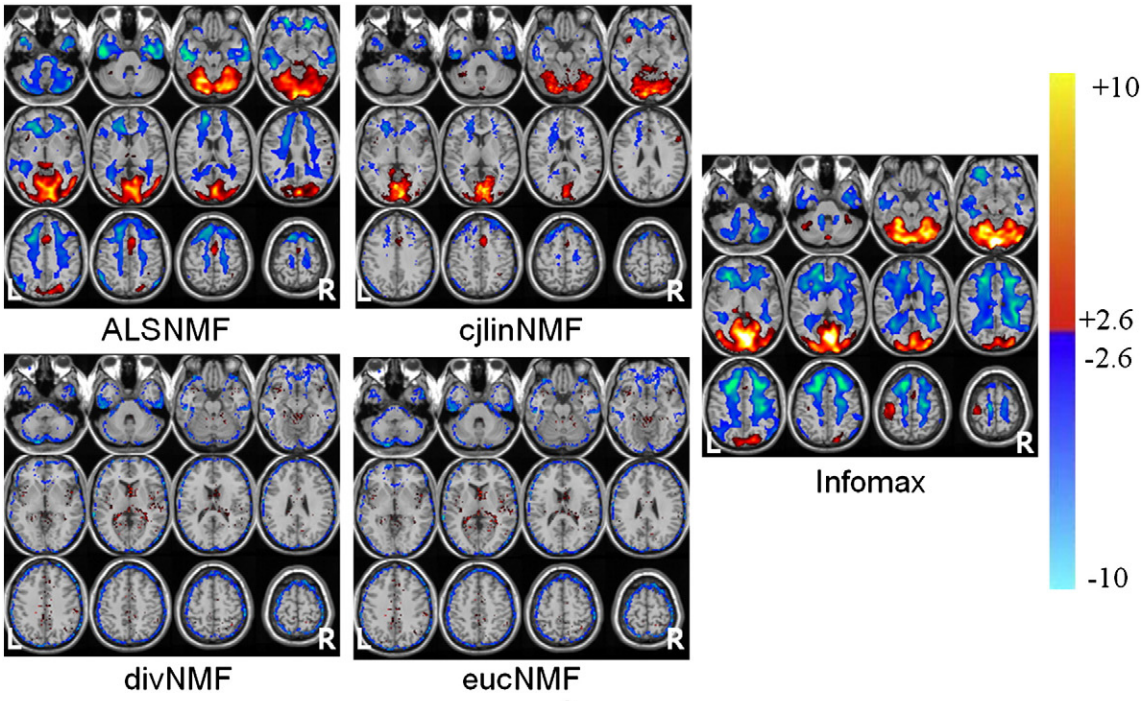

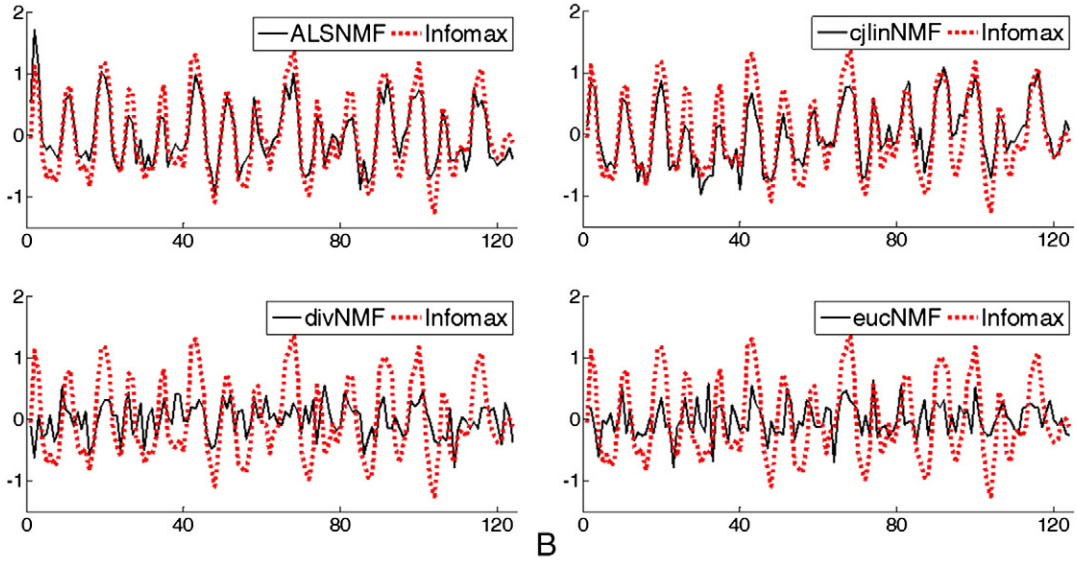

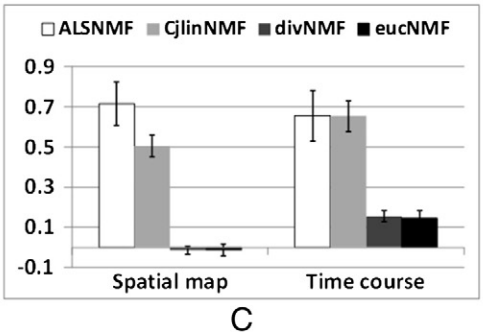

Fig. 6. Single-subject level results for fMRI data: (A) activation and deactivation maps of four NMFs and Infomax (reference) (uncorrected $P<.01$); (B) mean time courses of four NMFs; (C) Pearson's correlation of spatial and temporal patterns from each subject with the reference.

Table 2
Number of voxels (only activation) in estimated task-related components that overlapped with the BA masks

		Left somatosensory and motor area mask					Visual area mask		
		BA 1	BA 2	BA 3	BA 4	BA 6	BA 17	BA 18	BA 19
Single-subject level (P<.01)	ALSNMF	0	4	0	0	128	934	2373	1946
	cjlinNMF	0	1	0	0	40	807	1659	853
	Infomax	11	45	125	138	136	948	2398	1994
Group level (|z|>1.5)	ALSNMF	0	0	0	0	2	732	1854	1189
	cjlinNMF	3	58	130	153	268	142	263	172
	Infomax	4	6	46	80	30	582	1297	791

area. The NMF and Infomax results were compared to these BA masks to calculate the overlap in number of voxels.

3. Experimental results and analysis

3.1. Results on simulated data

Fig. 4A–D shows the task-related activation and deactivation detected from t-score images by each NMF algorithm (P<1e−5), as well as the mean time courses calculated from 15 subjects' zero-mean unit-variance time courses. The least-squares update NMFs (i.e., ALSNMF and cjlinNMF) detected more integrated activation and deactivation than the multiplicative update NMFs (i.e., divNMF and eucNMF). Moreover, the time courses estimated by ALSNMF showed less distortion than that obtained by the other three NMF algorithms. As Pearson's correlation coefficient of each subject's spatial maps and time courses was calculated with the references (i.e., the simulated spatial and temporal patterns), Fig. 4E exhibits the mean and standard deviation of all the subjects' correlation coefficients. It indicates that the least-squares update NMFs (i.e., ALSNMF and cjlinNMF) surpass the multiplicative update NMF algorithms (i.e., divNMF and eucNMF) with higher correlation and lower standard deviation in decomposition of spatial maps, which is more important as our experimental target is to estimate spatial activation and deactivation.

Fig. 5 is the group-level results of detected activation and deactivation, which are thresholded at |z|>2.0 on the z-scored spatial maps. Among these four NMF algorithms, the activation and deactivation estimated by ALSNMF were the most comparable to the original source and contained less artifacts compared to that obtained by the other three NMFs. Although the time courses estimated by ALSNMF were not the most superior one, its spatial maps displayed the highest correlation with the reference of both tasks (see Table 1).

Table 3
Two-sample t test on mean and standard deviation of correlation between ALSNMF and cjlinNMF

	Mean	Standard deviation
Spatial map	ALSNMF>cjlinNMF at P<2.6e−6	No significant difference
Time course	No significant difference	ALSNMF>cjlinNMF at P<.005

3.2. Results on fMRI data

The results of the single-subject level analysis on fMRI data are displayed in Fig. 6 with the activation and deactivation thresholded at uncorrected P<.01. They indicate that the multiplicative update NMFs (i.e., divNMF and eucNMF) failed to accurately detect visuomotor task-related neuronal activities. The estimated statistically significant voxels showed randomly distributed patterns, which have no direct relation with the adopted visuomotor task paradigm. The least squares NMFs (i.e., ALSNMF and cjlinNMF) revealed the task-related activation. Since the activation is more meaningful than the deactivation for the visuomotor task, we mainly investigated the detected activation. For ALSNMF, cjlinNMF and Infomax, the number of active voxels that overlapped with the BA masks was calculated and displayed in Table 2. Although the activation in the visual area seemed similar for all these three algorithms, ALSNMF's result was more comparable with that of Infomax. Moreover, it contained fewer artifacts, such as the activation in insula and right-side inferior frontal gyrus implied by cjlinNMF. However, ALSNMF and cjlinNMF mainly detected the supplementary motor area (SMA) as the motor task-related active brain region, whereas Infomax found motor activation not only in SMA but also in the left-side primary motor cortex (PMC), which is a more dominant motor area for motor tasks involving the right index finger.

For the least-squares update NMF algorithms (i.e., ALSNMF and cjlinNMF) that detected visuomotor task-related neuronal activities, an additional reproducibility test was performed in which these two algorithms were executed 20 times on each subject's fMRI data. The mean and standard deviation of the spatial and temporal patterns' correlation with the reference (i.e., the spatial map and time course obtained by Infomax) are presented in Fig. 7. Then a two-sample t test was performed on these mean values and standard deviations (shown in Table 3). Although ALSNMF has a higher standard deviation in the time courses' correlation, implying that its reproducibility in extracting time courses is slightly deficient compared to cjlinNMF, the spatial maps obtained by ALSNMF present much higher correlation than that achieved by using cjlinNMF, which is more significant because our main goal is to estimate neuronal activities.

Fig. 8 exhibits the group-level results for 14 subjects' temporally concatenated BOLD matrix (|z|>1.5 on the z-scored spatial maps).

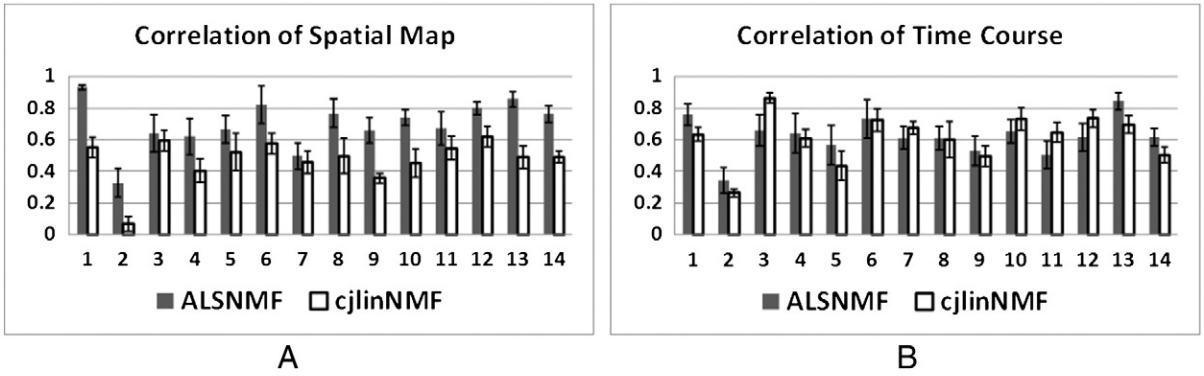

Fig. 7. Correlation bars of reproducibility test for (A) spatial maps and (B) time courses.

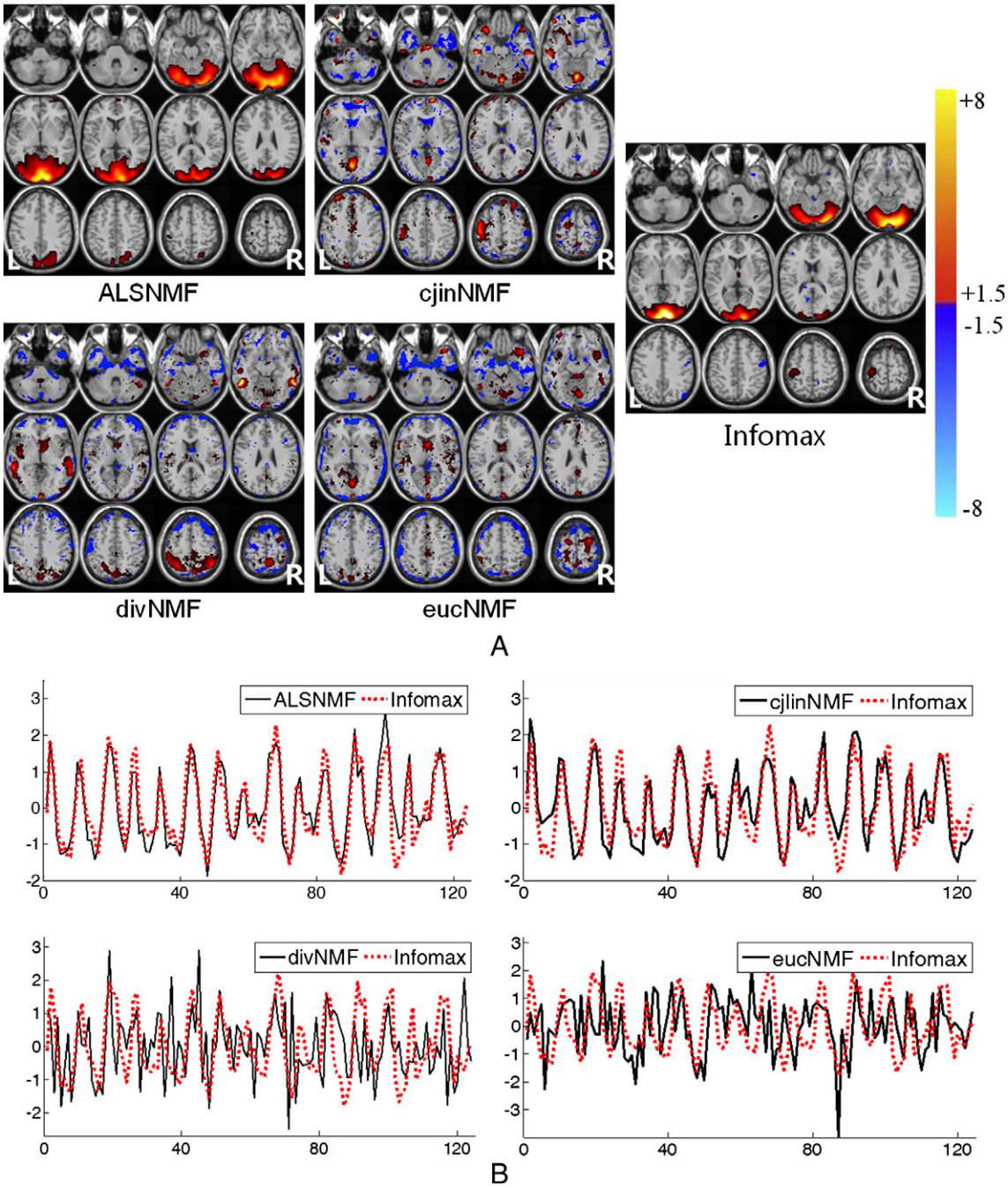

Fig. 8. Group-level results for fMRI data: (A) activation and deactivation maps of four NMFs and Infomax (reference) ($|z|>1.5$); (B) time courses of four NMFs.

Multiplicative update NMFs (i.e., divNMF and eucNMF) still fail to correctly estimate the task-related neuronal activities. For ALSNMF, cjlinNMF and Infomax, the number of active voxels that overlapped with the BA masks was calculated and displayed in Table 2 as well. ALSNMF's result was still the most comparable with that of Infomax, except that it only found slight activation in the left PMC. The spatial map of cjlinNMF was greatly inferior to that at the single-subject level, in which the presented activation in the visual area was widely different from the reference. However, it indicated the task-related activation in the left PMC, which might cause the time course to still have a high correlation with the reference (see Table 4).

Table 4
Pearson's correlation of spatial map and time course with the reference for each NMF algorithm in the group analysis of fMRI data

	ALSNMF	cjlinNMF	divNMF	eucNMF
Spatial map	0.8650	0.1443	0.0896	0.0151
Time course	0.9038	0.8440	0.3218	0.2356

4. Discussion

In this study, we explored the feasibility of different NMF algorithms performing BSS in order to estimate task-related neuronal activities from fMRI data, which has not been investigated before. We implemented four types of NMF algorithms, corresponding to two groups of update rules (i.e., least-squares update rules and multiplicative update rules), on simulated data and visuomotor task

fMRI data. We first tested them in single-subject level analysis and then measured their performance at the group level by temporally concatenating each subject's data.

NMF algorithms have the common property in that the input data matrix, decomposed weight matrix and basis matrix are all nonnegative. This property corresponds with the fact that fMRI data are nonnegative. From the point of view of neuroscience, the firing rates of neurons are never negative, and also synaptic strengths remain positive. This virtue appears obvious if NMF is modeled as a neural network. NMF executes BSS directly without any preprocessing procedures and decomposes the original data into feature-based meaningful parts. In the fMRI experiment, the task-related neuronal activities cause different BOLD signal changes in related voxels, which can be treated as features in NMF. As described in the previous section, although the decomposed spatial map matrix and time course matrix are both nonnegative, they can be viewed as positive baseline's biased matrices. After subtracting the baseline from corresponding spatial map, the spatial map will have both positive and negative values containing activation as well as deactivation. In this case, it is reasonable to apply NMF in the fMRI data analysis.

Least-squares update NMF algorithms (i.e., ALSNMF and cjlinNMF) seem to have the capability of estimating neuronal activities. In single-subject level analysis, both ALSNMF and cjlinNMF detected meaningful neuronal activities through BSS. However, the performance of cjlinNMF declined obviously in group-level analysis on real fMRI data. One possible reason for this is that cjlinNMF is sensitive to the initialization of weight matrix **W** and basis matrix **H** [30]. This weakness may become critical when using a data set with a huge size. In cjlinNMF's training process, it will terminate once it has satisfied the termination condition that each updating term of the parameters (i.e., the second half of Eq. (4)) is less than a threshold. For a huge data set, it probably terminates at a point that is not very far from the initial matrix. The initialization of **W** and **H** also has an influence on ALSNMF's outcome, which is revealed by the reproducibility test. In order to eliminate this effect in the ALSNMF decomposition, we can take some approaches, such as executing it several times and doing a random-effect analysis. Besides, in ALSNMF, the updating of one parameter has no direct relationship with its current value in a present iteration. It only depends on the original input data and another parameter matrix. This property allows ALSNMF to escape from a poor path during the iterative process and avoids convergence near the initialization points.

The group of multiplicative update NMF algorithms (i.e., eucNMF and divNMF) presented tolerable results for simulated data, but failed to estimate task-related activation for real fMRI data. In Ref. [31], it is mentioned that this group of NMF algorithms may converge to a stationary point which is not the local minimum. The risk that the algorithms cannot converge to a local minimum point is probably much higher for large data sets such as the raw BOLD fMRI matrix. Also, it possibly causes a substantial residual error for high-dimensional data sets as mentioned in Ref. [32]. Moreover, Plis et al. [33] showed that correlated noise would make multiplicative update NMF algorithms fail to decompose the data, which may be the case for the real fMRI data.

In this experiment, we used the modeled regressor to select the task-related component. In the single-subject analysis, the right finger-related motor activation detected by NMF was mainly located in SMA, which was not accordant with the ICA result and experiential knowledge that it should have the left PMC activation as well. For this point, we inspected the selected NMF component for each individual. For some subjects, the selected components contained the left PMC activation, but for the others, the left PMC showed activation in the unselected components, which caused the final *t*-map containing no left PMC activation at the defined threshold. Although there is still no direct evidence that NMF approach can be beyond ICA methods in the analysis of task-related fMRI data, our work may point out an alternative multivariate analysis approach. Since the NMF does not have any stringent assumption on the obtained components, it is believable that the performance of ALSNMF still has space to be improved [19]. For our experiment, it is possible that the activation in the left PMC might be well detected in the task-related component if some additional constraints are added during the training process.

Another potentially important issue is that, in practice, it is critical to make an appropriate decision on the number of components in the NMF decomposition, and the choice is very often problem dependent. In our experiment, we set the component number to 3 for the simulated data according to our prior knowledge. For the fMRI data, the number was set to 10 by drawing on experience for the single-subject data and it was evaluated to be 29 by MDL criteria for group data. We chose these values based on the reason that a much smaller number may cause incomplete decomposition and a much larger one will possibly split the integrated components. However, evaluating the NMF decomposition result according to the number of components, as well as finding proper criteria for component number setting, will be an interesting topic for future research. Also, the problem that the activation in the left PMC was not contained in selected task-related spatial maps for some subjects might be improved with a different setting of the component number.

5. Conclusion and further research

We did an exploratory experiment that evaluated the performance of four different NMF algorithms in estimating task-related neuronal activities from fMRI data. The result showed that least-squares update NMF algorithms (i.e., ALSNMF and cjlinNMF) worked well on single-subject data. At the group level, ALSNMF outperformed cjlinNMF in detecting neuronal activities. In comparison, multiplicative update NMF algorithms (i.e., divNMF and eucNMF) performed much worse in that they failed to accurately find the task-related brain regions. In brief, ALSNMF may be the most viable and useful NMF algorithm in the context of estimating task-related neuronal activities from fMRI data. The aim of our further research will be to improve ALSNMF, to make it more applicable in the field of estimating neuronal activities from fMRI data.

References

[1] Friston KJ, Holmes AP, Worsley KJ, Poline JP, Frich CD, Frackowiak RSJ. Statistical parametric maps in functional imaging: a general linear approach. Hum Brain Mapp 1995;2:189-210.
[2] Viviani R, Grön G, Spitzer M. Functional principal component analysis of fMRI data. Hum Brain Mapp 2005;24:109-29.
[3] McKeown MJ, Makeig S, Brown GG, Jung TP, Kindermann SS, Bell AJ, et al. Analysis of fMRI data by blind separation into independent spatial components. Hum Brain Mapp 1998;6:160-88.
[4] Lee JH, Lee TW, Jolesz FA, Yoo SS. Independent vector analysis (IVA): multivariate approach for fMRI group study. Neuroimage 2008;40:86–109.
[5] Li YO, Adalı T, Wang W, Calhoun VD. Joint blind source separation by multiset canonical correlation analysis. IEEE Trans Signal Proces 2009;57:3918-29.
[6] Calhoun VD, Adalı T, Pearson GD, Pekar JJ. A method for making group inference from functional MRI data using independent component analysis. Hum Brain Mapp 2001;14:140-51.
[7] McKeown MJ, Jung TP, Makeig S, Brown G, Kindermann SS, Lee TW, et al. Spatially independent activity patterns in functional MRI data during the Stroop color-naming task. Proc Natl Acad Sci U S A 1998;95:803-10.
[8] Calhoun VD, Adali T, McGinty VB, Pekar JJ, Watson TD, Pearlson GD. fMRI activation in a visual-perception task: network of areas detected using the general linear model and independent component analysis. Neuroimage 2001;14:1080-8.
[9] Chen S, Ross TJ, Zhan W, Myers CS, Chuang KS, Heishman SJ, et al. Group independent component analysis reveals consistent resting-state networks across multiple sessions. Brain Res 2008;1239:141-51.

[10] Correa N, Adalı T, Calhoun VD. Performance of blind source separation algorithms for fMRI analysis using a group ICA method. Magn Reson Imaging 2007;25:684-94.
[11] Langers DRM. Blind source separation of fMRI data by means of factor analytic transformations. Neuroimage 2009;47:77-87.
[12] Daubechies I, Roussos E, Takerkart S, Benharrosh M, Golden C, D'Ardenne K, et al. Independent component analysis for brain fMRI does not select for independence. Proc Natl Acad Sci 2009;106:10415-22.
[13] Lee DD, Seung HS. Learning the parts of objects by non-negative matrix factorization. Nature 1999;401:788-91.
[14] Pascual-Montano A, Carazo JM, Kochi K, Lehmann D, Pascual-Marqui RD. Nonsmooth nonnegative matrix factorization (nsNMF). IEEE Trans PAMI 2006;28:403-15.
[15] Devarajan K. Nonnegative matrix factorization: an analytical and interpretive tool in computational biology. PLoS Comput Biol 2008;4:e1000029.
[16] Zheng CH, Ng TY, Zhang L, Shiu CK, Wang HQ. Tumor classification based on nonnegative matrix factorization using gene expression data. IEEE Trans Nanobiosci 2011;10:86-93.
[17] Lohmann G, Volz KG, Ullsperger M. Using non-negative matrix factorization for single-trial analysis of fMRI data. Neuroimage 2007;37:1148-60.
[18] Potluru VK, Calhoun VD. Group learning using contrast NMF: application to functional and structural MRI of schizophrenia. Proceedings of IEEE International Symposium on Circuits and Systems (ISCAS), Seattle, USA: IEEE; 2008. p. 1336-9, http://ieeexplore.ieee.org/xpls/abs_all.jsp?arnumber=4541673.
[19] Ding X, Lee JH, Lee SW. A constrained alternating least squares nonnegative matrix factorization algorithm enhances task-related neuronal activity detection from single subject's fMRI data. Proceedings of International Conference on Machine Learning and Cybernetics (ICMLC), Guilin, China: IEEE; 2011. p. 338-43, http://ieeexplore.ieee.org/xpls/abs_all.jsp?arnumber=6016680.
[20] Lee JH, Hashimoto R, Wible CG, Yoo SS. Investigation of spectrally coherent resting-state networks using non-negative matrix factorization for functional MRI data. Int J Imag Syst Tech 2011;21:211-22.
[21] Paatero P, Tapper U. Positive matrix factorization: a non-negative factor model with optimal utilization of error estimates of data values. Environmetrics 1994;5:111-26.
[22] Paatero P. Least squares formulation of robust non-negative factor analysis. Chemometr Intell Lab Syst 1997;37:23-35.
[23] Lee DD, Seung HS. Algorithms for non-negative matrix factorization. Adv Neural Info Proces Syst 2001;13:556-62.
[24] Lin CJ. Projected gradient methods for non-negative matrix factorization. Neural Comput 2007;19:2756-79.
[25] Hoyer PO. Non-negative matrix factorization with sparseness constraints. J Mach Learn Res 2004;5:1457-69.
[26] Cichocki A, Zdunek R. Regularized alternating least squares algorithms for non-negative matrix/tensor factorization. In: Liu D, editor. Lecture Notes in Computer Science (LNCS) 2007;4493:793-802.
[27] Cai D, He X, Han J, Huang TS. Graph regularized nonnegative matrix factorization for data representation. IEEE Trans PAMI 2011;33:1548-60.
[28] Buckner RL, Snyder AZ, Sanders AL, Raichle ME, Morris JC. Functional brain imaging of young, nondemented, and demented older adults. J Cogn Neurosci 2000;12:24-34.
[29] Li YO, Adali T, Calhoun VD. Estimating the number of independent components for functional magnetic resonance imaging data. Hum Brain Mapp 2007;28:1251-66.
[30] Berry MW, Browne M, Langville AN, Pauca VP, Plemmons RJ. Algorithms and applications for approximate nonnegative matrix factorization. Comput Stat Data Anal 2007;52:155-73.
[31] Lin CJ. On the convergence of multiplicative update algorithms for nonnegative matrix factorization. IEEE Trans Neural Networks 2007;18:1589-96.
[32] Cichocki A, Zdunek R, Amari SI. Nonnegative matrix and tensor factorization. IEEE Signal Proc Mag 2008;25:142-5.
[33] Plis SM, Potluru VK, Lane T, Calhoun VD. Correlated noise: how it breaks NMF, and what to do about it. J Signal Process Syst 2011;65:351-9.